

Recycling of Secondary Aluminum Dross to Fabricate Porous γ -Al₂O₃ Assisted by Corn Straw as Biotemplate

Senjing Zhang, Weijun Zhu, Qingda Li, Wenjie Zhang, Xuemei Yi*

College of Mechanical and Electronic Engineering, Northwest A&F University, Yangling, China

Email: *xuemei_yi@nwsuaf.edu.cn

How to cite this paper: Zhang, S.J., Zhu, W.J., Li, Q.D., Zhang, W.J. and Yi, X.M. (2019) Recycling of Secondary Aluminum Dross to Fabricate Porous γ -Al₂O₃ Assisted by Corn Straw as Biotemplate. *Journal of Materials Science and Chemical Engineering*, 7, 87-102.

<https://doi.org/10.4236/msce.2019.712010>

Received: November 13, 2019

Accepted: December 27, 2019

Published: December 30, 2019

Copyright © 2019 by author(s) and Scientific Research Publishing Inc. This work is licensed under the Creative Commons Attribution International License (CC BY 4.0).

<http://creativecommons.org/licenses/by/4.0/>



Open Access

Abstract

In the aluminum industry, secondary aluminum dross (SAD) is an inevitable solid residue, which usually contains 30 - 70 wt% Al₂O₃. In this work, Al(OH)₃ was extracted from SAD through acid-leaching and alkali purification process. The as-obtained Al(OH)₃ precipitation then was calcinated to synthesize porous γ -Al₂O₃ assisting by an agricultural waste biomass-corn straw as biotemplate. Effects of H₂SO₄ concentration, reaction temperature and time on the recovery of SAD were investigated. Furthermore, the dependence of calcination temperature on specific surface area, pore volume and content of porous γ -Al₂O₃ was analyzed. X-ray diffraction (XRD) and X-ray fluorescence (XRF) were used to inspect the phase compositions and their contents, respectively. Scanning electron microscopy (SEM) was employed to analyze the morphologies of the sintered porous γ -Al₂O₃. It was found that the highest recycle rate of aluminum from SAD was obtained under optimum conditions of 80°C, acid concentration of 1.6 mol/l, and reaction time of 5 h by acid process. The porous γ -Al₂O₃ with specific surface area, 261.22 m²/g and average pore diameter, 52.64 nm, was obtained under calcination at 850°C through mixing the as-obtained Al(OH)₃ precipitation and corn straw.

Keywords

Secondary Aluminum Dross, Purification, Biotemplate, Corn Straw, Al₂O₃

1. Introduction

Aluminum dross is the molten slag solid waste that results from the production and recycling process of electrolytic aluminum, cast aluminum and other aluminum industries [1] [2] [3]. The composition of aluminum dross is very complex. Its main components are aluminum oxide and ferric oxide (Al₂O₃, Fe₂O₃),

silicon dioxide (SiO_2), spinel ($\text{MgO}\cdot\text{Al}_2\text{O}_3$), and some amount of fluoride and chloride compounds [4] [5]. To date, the treatment of aluminum dross waste mainly consists of accumulation in landfills, which not only seriously pollutes the environment, but is also a waste of aluminum resources [6] [7] [8] [9]. Hence, efficient recycling procedures for aluminum dross are an urgent necessity.

Presently, the extraction of alumina products from aluminum dross is a predominant implementation for efficient aluminum resource utilization [10]. Furthermore, aluminum dross can be divided into primary and secondary aluminum dross (SAD), depending on its recycling process times and its metallic aluminum content. Unfortunately, it is difficult to extract metal aluminum from SAD due to too low content [11] [12] [13]. Elemental aluminum extraction methods mainly include acid (sulfuric acid method, hydrochloric acid method) and alkaline leaching method, whereby the purpose is to separate the elemental aluminum from other impurities [14]. Dash *et al.* studied alumina recovery from aluminum dross using H_2SO_4 and found that more than 85% of alumina could be dissolved by leaching with 30% H_2SO_4 and 10% solid concentration at 363 K (90°C) for 1 h [15]. Md. Saifur Rahman Sarker *et al.* Murayama *et al.* reported that the aluminum dross was leached with HCl and NaOH. Under optimal conditions (*i.e.* $C_{\text{HCl}} = 2.0$ mol/L, $C_{\text{NaOH}} = 2.0$ mol/L, $t = 5$ h), the maximum dissolved amount of aluminum dross was 65% and 36%, respectively. The filtrate obtained by purifying with NaOH had higher purity of Al (*i.e.* 96%), but the recovery of Al was lower compared with HCl leaching [16]. Tsakiridis *et al.* used a strong 260 g/L NaOH solution to leach out aluminum which reached 57.5% from aluminum black dross at 513 K (240°C) for 100 minutes; under those conditions about 28% of the residues were dissolved [17]. The possibility of acid leaching of aluminum dross was investigated by Md. Saifur Rahman Sarker *et al.*, where the maximum of alumina extraction (71 % of total Al_2O_3 content from aluminum dross) was achieved by leaching with a 4 mol/L HCl solution at 373 K (100°C) for 120 min [18]. In this study, H_2SO_4 was used; various parameters affected the amount of aluminum element leaching such as acid concentration, reaction temperature and reaction time, among others.

During the aluminum dross leaching stage, a filtrate could be rendered through optimal aluminum ion dissolution conditions; but the remaining Si, Ca, Mg and Fe metal ions still need to be purified [19]. Preparation of high purity aluminum hydroxide ($\text{Al}(\text{OH})_3$) is a prerequisite for the production of calcined alumina. Therefore, the excess NaOH reacts with aluminum sulfate ($\text{Al}_2(\text{SO}_4)_3$) contained in the filtrate to form sodium aluminate (NaAlO_2) dissolved in solution, while the other metal hydroxides remain as a precipitate. This preparation is then filtered to remove undissolved materials, adjusting the pH of the resulting filtrate to regenerate a high purity $\text{Al}(\text{OH})_3$ precipitation [20].

In addition to smelting metal aluminum, alumina has a wide variety of useful applications such as structural materials, refractories, catalysts and carriers [21].

Also, depending on the different formation temperatures, alumina can have different structures. Thus, alumina can be divided into low-temperature alumina (ρ -, χ -, η - and γ -Al₂O₃) and high-temperature alumina (δ -, κ - and θ -Al₂O₃) [22]. In particular, the low-temperature transition state γ -Al₂O₃ is porous, has high specific surface area, good adsorption, and thermal stability. γ -Al₂O₃ with different specific surface areas and porosity can be prepared by controlling the preparation conditions; however, consistent porosity is reportedly challenging to attain. For instance, some studies have found that alumina prepared by sintering at low temperature tends to agglomerate, lowering the specific surface area and average pore diameter of the product, and affecting the performance of the alumina as a carrier [23]. In contrast, Song *et al.* reported that the gas produced by sintering at low temperature can also expand the pore structure of alumina [24].

Corn straw is an agricultural byproduct and contains a large amount of cellulose, hemicellulose and lignin. Interestingly, its microstructure closely resembles a honeycomb. Here, our goal was to maximize the utilization of SAD to fabricate porous γ -Al₂O₃ assisting by corn straw as a sacrificial template through calcination, which could potentially be used for phase change materials (PCM) support.

2. Materials and Methods

2.1. Materials and Chemical Reagents

Secondary aluminum dross (SAD) was supplied by Delta Aluminum Industry CO., LTD located in Zhaoqing city, China. Sulphuric acid (H₂SO₄, 96% - 98% purity) and sodium hydroxide (NaOH, 99% purity) were used for acid extraction and alkali purification of SAD.

Table 1 shows the sample conditions, where A and B denote the samples before and after washing, respectively. The SAD contains soluble salts such as magnesium oxide, sodium oxide, chlorides and fluoride. To increase the aluminum leaching rate, the SAD requires to be washed with deionized water to remove the soluble impurities [25]. The 20 g of SAD was tread with 500 ml of deionized water, stirred and dissolved for 3 - 4 h, then filtered; the filter residue was placed in a vacuum oven at 110 °C for 3 h.

Figure 1 summarizes the experimental procedure. The SAD was first acidified to obtain filter residue and filtrate to determine the optimal experimental scheme. Then, the filtrate was purified through NaOH to prepare a high-purity Al(OH)₃ precipitation, finally the precipitation and straw powders were mixed and sintered.

Table 1. Chemical composition analysis of SAD before and after washing.

Composition	Al ₂ O ₃	MgO	SiO ₂	Na ₂ O	Fe ₂ O ₃	Cl	CaO	K ₂ O	F	CuO	Other
(A) Mass pct	73.14	7.00	4.27	3.59	3.31	2.95	1.53	0.78	0.75	0.61	2.07
(B) Mass pct	73.93	6.20	6.56	0.88	5.80	0.42	1.52	0.30	0.63	0.94	2.82

A: before washing B: after washing.

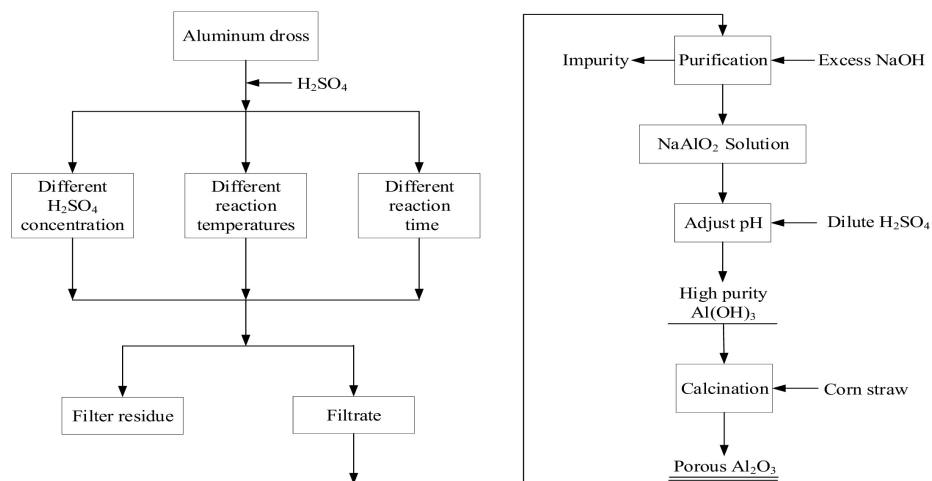


Figure 1. Flowchart on preparation of porous alumina from SAD.

2.2. Methods

2.2.1. Extraction of Aluminum by Acid Leaching Method

A total of 20 g of washed SAD were transferred to a flat-bottomed glass reactor, which in turn was placed in a thermostat water bath. The washed SAD was leached using different molar ratios of H_2SO_4 (1 - 1.8) for different periods of time (0.5 - 5 h) at different leaching temperatures ranging from 50 °C to 90 °C. Then, the mixture was stirred and filtered, collecting the filter residue and filtrate, after which the element content of the residue was measured by XRF.

2.2.2. Preparation of the $\text{Al}(\text{OH})_3$

Purification of the filtrate was performed by adding a 5N NaOH solution. Then, the pH of the filtrate was adjusted to prepare $\text{Al}(\text{OH})_3$ by diluting with H_2SO_4 , and the products were collected. However, the reaction was accompanied by a large amount of Na_2SO_4 . To remove Na_2SO_4 , the products were repeatedly washed with 500 ml deionized water using a magnetic stirrer equipment at 800 rpm for 30 minutes. A cerium chloride (BaCl_2) solution was dropped into the filtrate to check whether the Na_2SO_4 was completely removed. The collected high purity $\text{Al}(\text{OH})_3$ was placed in a vacuum oven, followed by drying at 110 °C for 12 h. Finally, the extracted powders were detected by X-ray diffraction (XRD) and X-ray fluorescence (XRF).

2.2.3. Synthesis of Porous Alumina

First, the corn straw was cut and shattered, 20 mesh powder particles were selected. Then the high-purity $\text{Al}(\text{OH})_3$ and the straw powder were further mixed with a magnetic stirrer at 800 rpm according to a certain mass ratio. Said mixture components (*i.e.* mass ratio) are summarized in **Table 2**.

Subsequently, the mixtures were loaded into an alumina crucible, and placed into an electric furnace. The furnace was then heated from ambient temperature to 500 °C, 600 °C, 700 °C, 800 °C, 900 °C at a heating rate of 5 °C/min, respectively. The samples were maintained for 2 h at the setting temperatures before cooling to ambient temperature in the furnace.

Table 2. Compositions of the initial reactants.

Samples	Al(OH) ₃ (mass %)	Straw powder (mass %)
S1	100	0
S2	96	4
S3	94	6
S4	92	8
S5	90	10

2.2.4. Characterization

The phase composition of the resulting material was performed using X-ray diffraction (XRD; X'Pert Pro MPD System) with Cu K α radiation. Chemical composition of the SAD sample and extracted alumina powders were analyzed using ED2000 X-ray fluorescence (XRF) analyzer (Oxford, England). The microstructures were observed via scanning electron microscopy (SEM, Nova 450 Nano). The Brunauer-Emmett-Teller (BET) surface area and pore volume were determined by Thermo Finnigan Sorptomatic Instrument model 1990 Series, and the pore size distribution was estimated by the Barrett-Joyner Halenda (BJH) method.

3. Result and Discussion

3.1. Acid Leaching Experiment

For each acid dissolution experiment, 20 g of washed sample was used. Variations on the H₂SO₄ molar ratio, and temperature were controlled to study the influence of each single factor on the leaching rate of aluminum. XRF method was used to measure the elemental content of the filter residue, and aluminum leaching rate (x) was evaluated by the following equation:

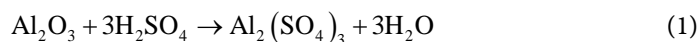
$$x = \frac{A_T - A_R}{A_T}$$

where, A_R (g) denotes the mass of elemental aluminum in the filter residue, and A_T (g) is the total mass of elemental aluminum in the washed SAD.

To evaluate the influence of H₂SO₄ molar mass on the leaching rate of elemental aluminum, the effect of different molar ratios was assessed from 1.0 to 1.8 mol/L. The leaching temperature was maintained at ambient temperature for 2 h.

The XRD pattern of SAD is shown in **Figure 2**. As can be seen, the main substance presents in SAD was Al₂O₃. Additionally, MgO, MgAl₂O₄, SiO₂, Fe₂O₃, CaO, CuO and CaF₂ were also present.

Due to the complex composition of the SAD, the potential chemical reactions in acid leaching process are as follows:



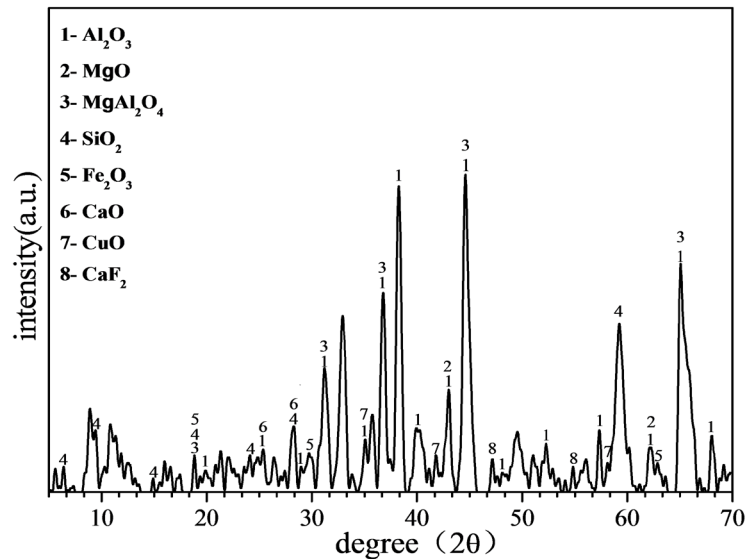


Figure 2. XRD pattern of SAD.

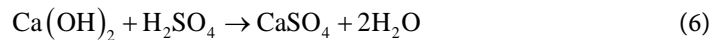
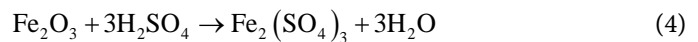
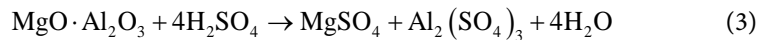


Figure 3(a) shows the effect of leaching time on aluminum element extraction for 1, 1.2, 1.4, 1.6, and 1.8 molar ratio of H_2SO_4 at ambient temperature. Elemental aluminum leaching rate increased overall with time under a 1.6 molar ratio. The highest leaching rate was observed from 0.5 to 1 h. As the molar ratio of H_2SO_4 increased to 1.6, the leaching rate of elemental aluminum was accelerated, but the further increase of the H_2SO_4 molar ratio to 1.8 lowered the leaching rate. The maximum leaching rate of 59.64% elemental aluminum was achieved with a 1.6 molar ratio of H_2SO_4 . Therefore, a 1.6 molar ratio of H_2SO_4 determined to be the optimum ratio for subsequent experiments.

Figure 3(b) shows the temperature-time profile for aluminum leaching rate at a 1.6 molar ratio. As can be seen, with increasing leaching temperatures, aluminum leaching rates exhibited an increasing trend. A maximum leaching rate of 70.7% elemental aluminum was obtained at 80°C . However, once the temperature reached 90°C , the aluminum leaching rate slowly decreased with time.

A SAD acidification process diagram is depicted in **Figure 4**. Here, the main purpose was to separate the soluble substances in the sulfuric acid from the insoluble solids. The acid leaching process may be mainly divided into three stages: 1) H_2SO_4 reacted mostly with the external surface of the SAD particle; 2) Under the action of H_2SO_4 decomposition and rapid stirring, H_2SO_4 diffused through

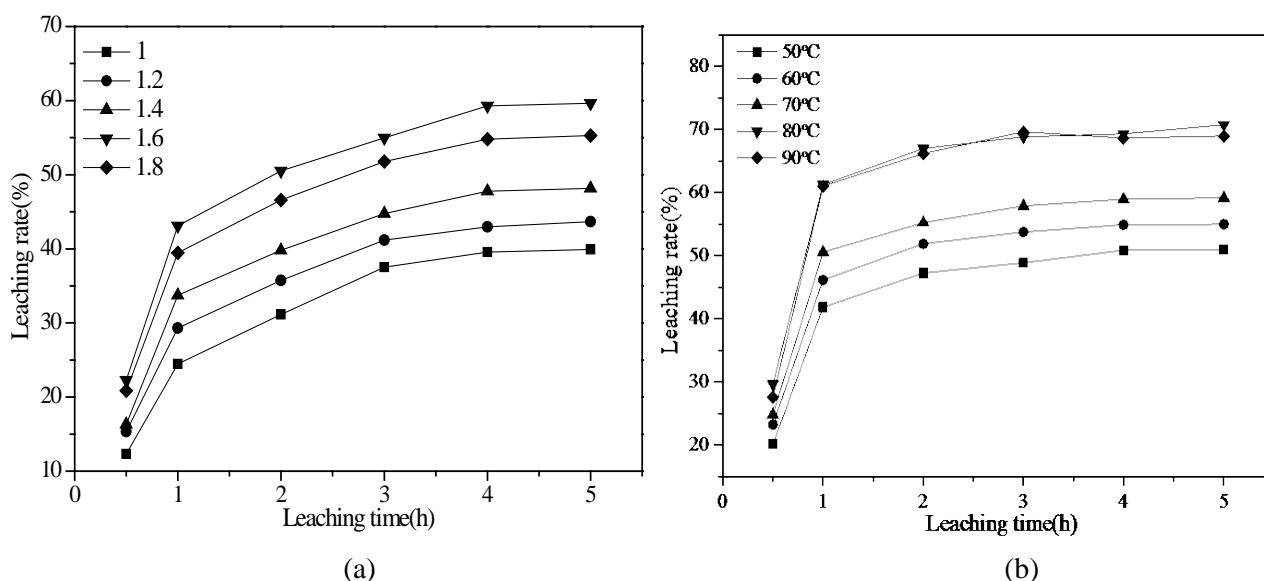


Figure 3. The acid leaching experiments of SAD. (a) Leaching rate of elemental aluminum at different H₂SO₄ molar ratio at ambient temperature; (b) Effect of temperature on the leaching rate of elemental aluminum at a 1.6 molar ratio.

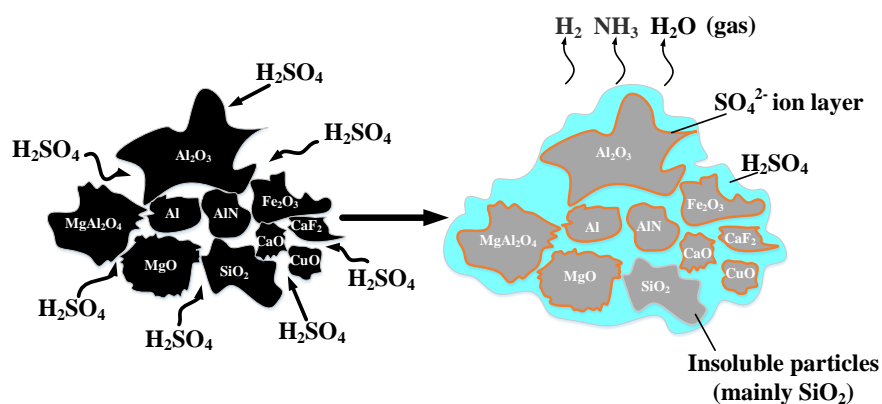


Figure 4. Schematic diagram of SAD acidification.

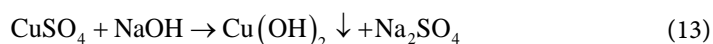
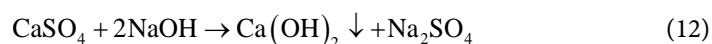
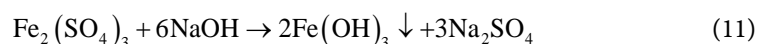
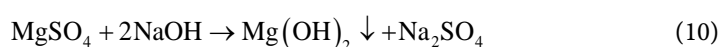
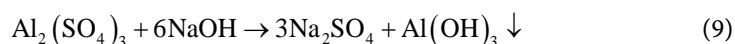
the particle gaps to the interior of the particle, and chemical reaction occurred at the contact interface; 3) A chemical reaction at the contact interface to produce a SO₄²⁻ ion layer, thereby forming a cycle of dissolution and sulfate generation.

The possible reasons for the decrease in the leaching rate of aluminum caused by excessive molar ratio (*i.e.* 1.8) and temperature (*i.e.* 90°C) are summarized in **Figure 4**. The reaction of SAD with H₂SO₄ is an exothermic reaction. Therefore, the heat generates a large amount of water vapor, releasing from the vessel, which causes the reaction volume to shrink and the concentration to rise. Excessive SO₄²⁻ ion concentration on the oxide surface produced a sulfate molecular layer, which may inhibit the chemical reaction. Additionally, increasing temperature accelerated the dissolution of the sulfate into solution, which confirmed, to a certain extent, that the leaching rate of aluminum is proportional to temperature. However, excess temperature could also cause evaporation of the water, which increased the concentration of SO₄²⁻ ions around the oxide.

The optimal acid leaching scheme in **Table 3** was obtained from sample prepared with a 1.6 molar ratio of H_2SO_4 at 80°C . Under this condition, the maximum leaching rate of elemental aluminum was 78.8%.

3.2. Purification of $\text{Al}(\text{OH})_3$

In order to obtain the maximum leaching rate of elemental aluminum, the optimal experimental scheme (1.6 molar ratio, 80°C) for the acid leaching procedure was selected. However, the filtrate mainly contained aluminum sulfate ($\text{Al}_2(\text{SO}_4)_3$), along with small amounts of other sulfate substances. Subsequently, the filtrate needed to be purified by NaOH solution. Possible chemical reaction schemes are indicated below.



In the process of $\text{Al}(\text{OH})_3$ preparation, the color of the product mainly appeared white at pH 7 - 8; however, the precursor color gradually deepened to reddish brown color at higher pH, see **Figure 5**. This indicated that the precursor preparation process contained more impurity components. Here, the main elements in the samples were oxygen, sodium, aluminum and sulfur. Furthermore, under higher pH, the aluminum content was decreased, which the content of other elements was increased (**Table 4**). According to Equation (14), the mainly reason was attributable to the reaction between $\text{Al}(\text{OH})_3$ with excess NaOH to form NaAlO_2 , then NaAlO_2 dissolved in the solution.

Table 3. XRF elemental analysis of SAD before and after reaction in a 1.6 molar ratio of H_2SO_4 at 80°C .

Elements	Al	O	S	Si	Mg	Cu	Fe	Ca	Other
Mass pct	18.76	58.24	11.9	4.74	2.29	1.01	0.98	0.43	1.65

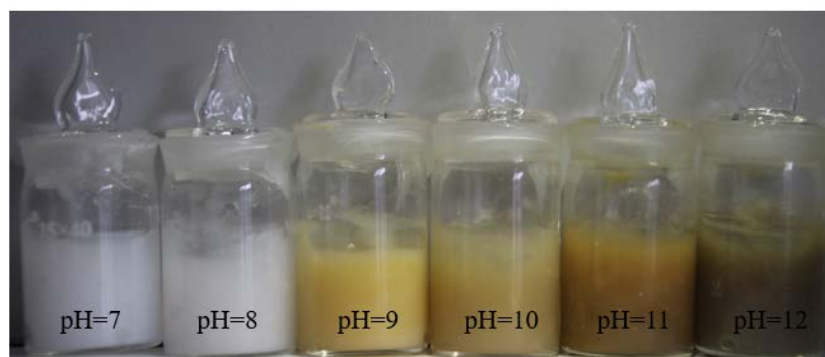
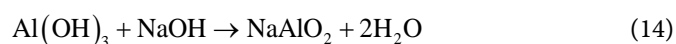


Figure 5. Resulting color variation of the precursor under different pH conditions.

Table 4. XRF elemental analysis of the precursors at different pH conditions.

Elements	Samples (Mass pct)					
	pH7	pH8	pH9	pH10	pH11	pH12
O	48.40	47.80	47.50	47.40	47.50	49.70
Na	19.70	20.70	22.00	23.40	24.70	25.70
Al	13.10	12.70	11.10	9.20	6.70	4.20
S	17.90	17.20	16.20	16.40	16.80	16.40
Mg	0.24	0.32	0.36	0.99	1.07	2.08
Ca	0.19	0.24	0.30	0.56	0.55	0.61
Si	0.03	0.03	0.03	0.19	0.16	0.26
Fe	0.20	0.55	0.72	0.72	0.74	0.86
Other	0.24	0.46	1.79	1.14	1.78	0.19



After removing impurities through filtration, the filtrate at pH 12 was selected to adjust pH 8 to regenerate the $\text{Al}(\text{OH})_3$ precipitation, and the main component of the sample was Na_2SO_4 and $\text{Al}(\text{OH})_3$. After washing several times, sodium sulfate content reduced a trace amount. Moreover, the aluminum and oxygen content reached 99.4% (**Figure 6** and **Table 5**).

3.3. Preparation of Porous Alumina

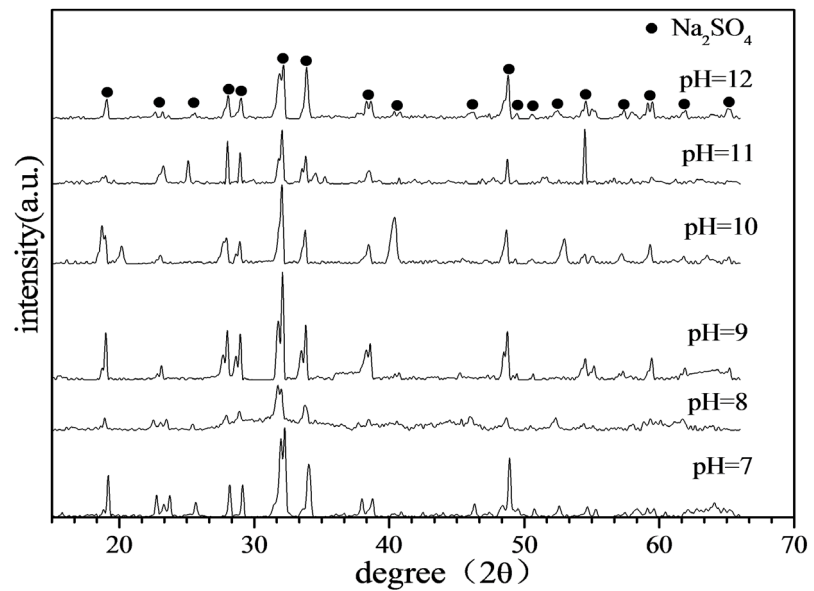
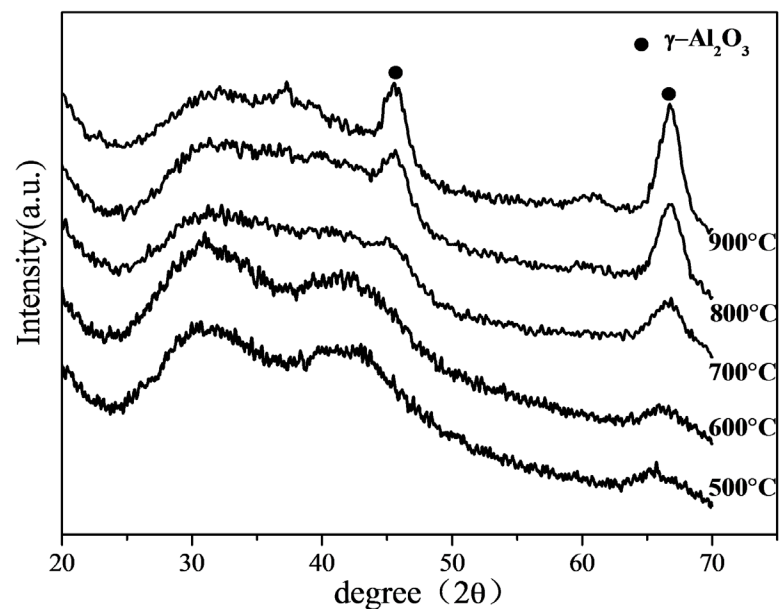
The XRD patterns in **Figure 7** were obtained from sample S1 calcined at the different temperatures. It indicated that $\gamma\text{-Al}_2\text{O}_3$ began to form when the temperature reached 700°C , and the products exhibited an amorphous nature when temperatures between 500°C and 600°C . Therefore, above 700°C were selected for subsequent sintering experiments.

Figure 8 shows XRD results of samples after calcined at 800°C for 2 h. The chemical compositions of samples are listed in **Table 3**. As seen in it, the strong peaks of the samples were all associated with $\gamma\text{-Al}_2\text{O}_3$, but with an increase of straw content, the intensity of weak peaks increased gradually. Moreover, the content of Al_2O_3 gradually decreased, the content of other substances increased, the maximum Al_2O_3 content was 93.9%. This indicated that the content of straw content had a significant impact to the purity of the product after sintering.

Figure 9 shows XRD results of different samples after calcined at 900°C for 2 h. It is easy to see that the strong peaks of the samples were also $\gamma\text{-Al}_2\text{O}_3$, and the chemical compositions of samples are illustrated in **Table 7**. It can be seen that the maximum Al_2O_3 content was 97.2%, the content of alumina gradually decreased, the content of other substances increased. However, compared with 800°C , the content of other substances was less, and the purity of the products was higher. This suggests that the elevated temperature could more thoroughly burn the straw powders, further increased the content of Al_2O_3 .

Table 5. XRF elemental analysis of the precursors at different pH conditions.

Element	Sample		
	First wash	Fifth wash	Tenth wash
O	47.3	50.9	63.2
Na	23.7	15.40	0.09
Al	10.6	20.3	36.20
S	18.0	13.0	0.26
Other	0.40	0.40	0.25

**Figure 6.** XRD results from the precursor obtained under different pH conditions.**Figure 7.** XRD results of sample S1 after calcined at different temperatures.

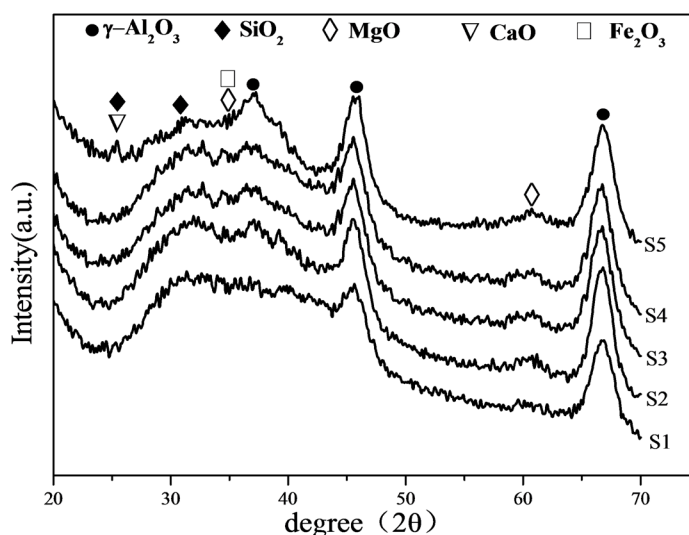


Figure 8. XRD results of different samples after calcined at 800°C for 2 h.

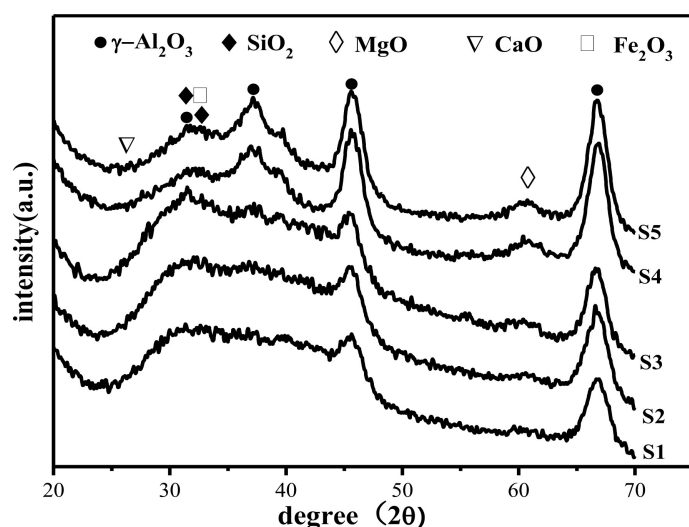


Figure 9. XRD results of different samples after calcined at 900°C for 2 h.

According to the analysis of **Table 6** and **Table 7**, the addition of straw content above 6% lead to an obviously decreased purity of the product. Therefore, 6% straw content was selected as the optimal scheme.

Figure 10 illustrates the N_2 adsorption-desorption isotherms and pore size distributions of the calcined samples. The curve bulged upward in the low pressure area, similar to the type II isotherm, which corresponded to the outer surface adsorption. The isotherms rose rapidly in the high pressure area with the appearance of hysteresis loops, indicating that the adsorbate began to undergo capillary condensation in the finest mesopores. These isotherms all display a classical IV type with hysteresis loops, which explained that the mesoporous portion was comprised of cracked holes [26].

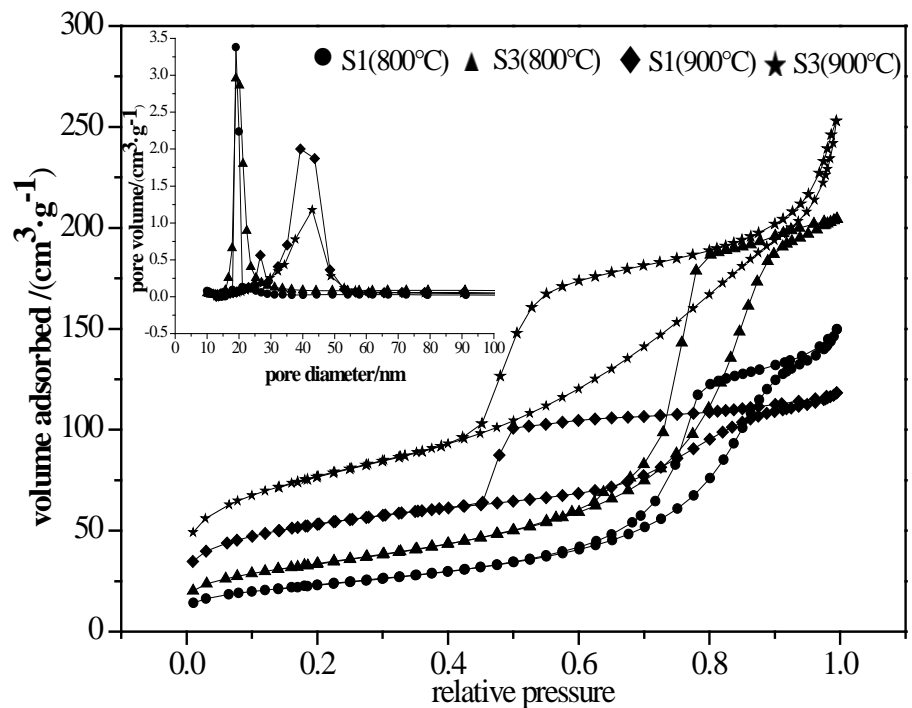
However, as the temperature increased, and the content of straw content increased, so did the starting point of the isotherm. Also, the starting point of the

Table 6. Chemical compositions of different samples after calcined at 800 °C for 2 h.

Chemical composition	Sample				
	S1 (%)	S2 (%)	S3 (%)	S3 (%)	S4 (%)
Al ₂ O ₃	93.9	88.9	88.6	85.2	84.0
SO ₃	5.18	6.17	6.34	6.68	7.76
SiO ₂	0.47	2.60	3.34	4.78	6.03
MgO	-	0.38	0.51	0.52	0.54
CaO	0.01	0.71	0.98	0.79	0.89
Fe ₂ O ₃	0.02	0.06	0.08	0.07	0.07
Other	0.42	1.18	0.15	1.96	0.71

Table 7. Chemical compositions of different samples after calcined at 900 °C.

Chemical composition	Sample				
	S1 (%)	S2 (%)	S3 (%)	S4 (%)	S5 (%)
Al ₂ O ₃	97.2	96.5	96.4	92.3	89.6
SO ₃	2.05	2.16	2.19	4.69	5.28
SiO ₂	0.51	0.64	1.02	1.65	2.96
MgO	-	0.16	0.12	0.13	0.29
CaO	0.03	0.29	0.13	0.27	0.56
Fe ₂ O ₃	0.04	0.04	0.03	0.04	0.03
Other	0.17	0.21	0.11	0.92	1.28

**Figure 10.** N₂ adsorption-desorption isotherm and pore size distribution.

hysteresis loop continued to advance. When the temperature increased to 900 °C and the content of the straw powders was 6%, the starting point of the isotherm, as well as the starting point of the hysteresis loop and the hysteresis loop itself all reached maximum values. The relative pressure was close to 1 Pa, the curve of sample S3 rose linearly and the adsorption was carried out on macropores, evidencing that the prepared sample had a macroporous structure.

All BET sample surface area, pore volume and average pore diameters were summarized in **Table 8**. Sample S1 exhibited a specific surface area of 80.06 m²/g, a pore volume of 0.22 cm³/g, and an average pore diameter of 105.51 nm. When adding 6% straw content to calcine at 800 °C, the pore volume, specific surface area and average pore diameter of sample S3 increased to 119.41 m²/g, 0.31 cm³/g, and 104.21 nm, respectively. This indicated that the gas produced by the straw powders during calcination could increase the specific surface area and pore volume of the sample, but the pore size was largely unchanged. Sample S1 was calcined at 900 °C, and the specific surface area, pore volume and average pore diameter of the sample were 176.92 m²/g, 0.18 cm³/g, and 40.23 nm, respectively.

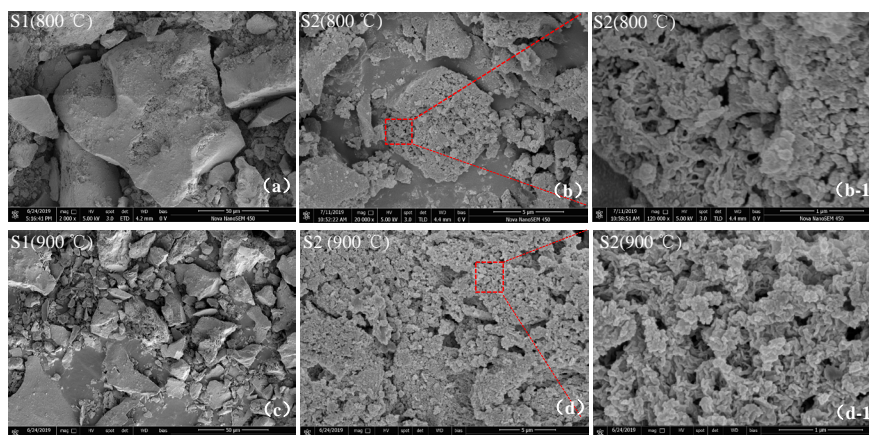
Compared with S1 (800 °C), the specific surface area of the sample S1 (900 °C) increased, and the pore volume and pore diameter decreased, this may be explained by an increased density of alumina due to the elevated temperature. Adding 6% straw powders to calcine at 900 °C, the pore volume, specific surface area and average pore diameter of sample S3 (900 °C) increased to 261.22 m²/g, 0.34 cm³/g, and 52.64 nm, respectively. Compared with S3 (800 °C), the specific surface area and pore volume of the sample increased, but the pore size decreased. High temperature promoted the rapid combustion of straw powders leading to a large amount of carbon dioxide production, This, in turn, caused alumina to produce a large number of micropores, which were then the widened to form a small number of mesopores and macropores. Compared with sample S1 (900 °C), the specific surface area, pore volume, and pore size of the sample all increased.

The morphology of the samples S1 and S3 was further investigated through SEM. **Figure 11(a)** and **Figure 11(c)** show the morphologies of the sample S1 at 800 °C and 900 °C, respectively. It can be observed that the morphologies of the sample had a large block structure at 800 °C, whereas at 900 °C, it had a small block structure. Therefore, the specific surface area was increased, which was consistent with the BET detection results. **Figure 11(b)** and **Figure 11(d)** show the morphologies of the sample S3 at 800 °C and 900 °C, respectively. The image showed that a large number of pores were formed on the surface of the block structure, which indicated that the straw powders promoted the formation of porous alumina, and increased the specific surface area and pore volume. The partial enlarged view in **Figure 11(b-1)**, **Figure 11(d-1)** further demonstrated that the surface of the product formed a uniform pore structure.

In conclusion, we extracted alumina from secondary aluminum dross and

Table 8. BET sample surface area, pore volume (V_p) and average pore diameter (D_p).

Samples	S_{BET} (m^2/g)	V_p (cm^3/g)	D_p (nm)
S1 (800 °C)	80.06	0.22	105.51
S3 (800 °C)	119.41	0.31	104.21
S1 (900 °C)	176.92	0.18	40.23
S3 (900 °C)	261.22	0.34	52.64

**Figure 11.** SEM images of samples heated for 2 h at 800 °C and 900 °C: (a) S1 (800 °C), (c) S1 (900 °C), (b) S3 (800 °C), (d) S3 (900 °C); (b-1) and (d-1) are partial enlargements

successfully used corn straw as template to prepare porous alumina. The influence mechanism of corn straw on alumina pore formation still needs further study.

4. Conclusion

Porous γ - Al_2O_3 was successfully fabricated by recovering secondary aluminum dross assisted by corn straw as template. First, a maximum 78.8% of aluminum was extracted from secondary aluminum dross at optimum conditions of 1.6 mol/l H_2SO_4 , 5 h leaching time, and a temperature of 80 °C. Second, high purity of 99.4% amorphous $Al(OH)_3$ was obtained after treating the acid leached solution with NaOH. Then, this $Al(OH)_3$ precipitate was mixed with 6% corn straw powders, and heat treated at 850 °C to obtain porous γ - Al_2O_3 . The final as-synthesized γ - Al_2O_3 had a specific surface area of 261.22 m^2/g , total pore volume of 0.34 cm^3/g , and average pore diameter of 52.64 nm, which can potentially be used for phase change materials (PCM) support.

Acknowledgements

This work was financially supported by Shaanxi Key R&D Program (No. 2018GY-116) and by Yangling Demonstration Zone Science and Technology Plan Project, Shaanxi, China (No. 2018GY-05).

Conflicts of Interest

The authors declare no conflicts of interest regarding the publication of this paper.

References

- [1] Zhang, J., Li, H.B. and Duan, Y.H. (2016) A Facile and Reliable Preparing Route of Brown Fused Alumina from Aluminum Dross. *Key Engineering Materials*, **680**, 335-338. <https://doi.org/10.4028/www.scientific.net/KEM.680.335>
- [2] Inegbenebor, A.O., *et al.* (2018) Assessment of Some Clay South West and Aluminium Dross as Roofing Tile Materials. *IOP Conference Series: Materials Science and Engineering*, **391**, Article ID: 12009. <https://doi.org/10.1088/1757-899X/391/1/012009>
- [3] Saravanakumar, R., Ramachandran, K., Laly, L.G., Ananthapadmanabhan, P.V. and Yugeswaran, S. (2018) Plasma Assisted Synthesis of γ -Alumina from Waste Aluminium Dross. *Waste Management*, **77**, 565-575. <https://doi.org/10.1016/j.wasman.2018.05.005>
- [4] Mohamad Zulfika, H.B.Z., Baini, R. and Ahmad Zauzi, N.S. (2017) Effect of pH, Dosage and Concentration on the Adsorption of Congo Red onto Untreated and Treated Aluminium Dross. *IOP Conference Series: Materials Science and Engineering*, **205**, Article ID: 12026. <https://doi.org/10.1088/1757-899X/205/1/012026>
- [5] Zulfika Hazielim, B., Zakaria, M., Baini, R., Sutan, N.M. and Rahman, R. (2017) Evaluation of Aluminium Dross as Adsorbent for Removal of Carcinogenic Congo Red Dye in Wastewater. *IOP Conference Series: Materials Science and Engineering*, **216**, Article ID: 12003. <https://doi.org/10.1088/1757-899X/216/1/012003>
- [6] EI Katatny, E.A., Halawy, S.A., Mohamed, M.A. and Zaki, M.I. (2000) Recovery of High Surface Area Alumina from Aluminium Dross Tailings. *Journal of Chemical Technology & Biotechnology*, **75**, 394-402. [https://doi.org/10.1002/\(SICI\)1097-4660\(200005\)75:5<394::AID-JCTB216>3.0.CO;2-7](https://doi.org/10.1002/(SICI)1097-4660(200005)75:5<394::AID-JCTB216>3.0.CO;2-7)
- [7] Sifontes, Á.B., *et al.* (2014) Preparation of Functionalized Porous Nano- γ -Al₂O₃ Powders Employing Colophony Extract. *Biotechnology Reports*, **4**, 21-29. <https://doi.org/10.1016/j.btre.2014.07.001>
- [8] Roth, D.J. (2011) The Approach to Zero Waste from Smelter and Secondary Dross Processing. *Materials Science Forum*, **693**, 24-32. <https://doi.org/10.4028/www.scientific.net/MSF.693.24>
- [9] Mailar, G., *et al.* (2016) Investigation of Concrete Produced Using Recycled Aluminium Dross for Hot Weather Concreting Conditions. *Resource-Efficient Technologies*, **2**, 68-80. <https://doi.org/10.1016/j.refit.2016.06.006>
- [10] Chang, J., Olivetti, E., Fjeldbo, S.K. and Kirchain, R. (2015) Data Mining toward Increased Use of Aluminum Dross. *Journal of Sustainable Metallurgy*, **1**, 53-64. <https://doi.org/10.1007/s40831-014-0003-3>
- [11] Hong, J., *et al.* (2010) Process of Aluminum Dross Recycling and Life Cycle Assessment for Al-Si Alloys and Brown Fused Alumina. *Transactions of Nonferrous Metals Society of China*, **20**, 2155-2161. [https://doi.org/10.1016/S1003-6326\(09\)60435-0](https://doi.org/10.1016/S1003-6326(09)60435-0)
- [12] David, E. and Kopac, J. (2013) Aluminum Recovery as a Product with High Added Value Using Aluminum Hazardous Waste. *Journal of Hazardous Materials*, **261**, 316-324. <https://doi.org/10.1016/j.jhazmat.2013.07.042>
- [13] Dai, C. and Apelian, D. (2017) Fabrication and Characterization of Aluminum Dross-Containing Mortar Composites: Upcycling of a Waste Product. *Journal of Sustainable Metallurgy*, **3**, 230-238. <https://doi.org/10.1007/s40831-016-0071-7>
- [14] Adeosun, S.O., Sekunowo, O.I., Balogun, S.A. and Obembe, O.O. (2012) Study on the Mechanical Properties of Cast 6063 Al Alloy Using a Mixture of Aluminum

- Dross and Green Sand as Mold. *JOM*, **64**, 905-910.
<https://doi.org/10.1007/s11837-012-0389-y>
- [15] Dash, B., Das, B.R., Tripathy, B.C., Bhattacharya, I.N. and Das, S.C. (2008) Acid Dissolution of Alumina from Waste Aluminium Dross. *Hydrometallurgy*, **92**, 48-53. <https://doi.org/10.1016/j.hydromet.2008.01.006>
- [16] Murayama, N., *et al.* (2012) Synthesis of Various Layered Double Hydroxides Using Aluminum Dross Generated in Aluminum Recycling Process. *International Journal of Mineral Processing*, **110-111**, 46-52.
<https://doi.org/10.1016/j.minpro.2012.03.011>
- [17] Tsakiridis, P.E., Oustadakis, P. and Agatzini-Leonardou, S. (2013) Aluminium Recovery during Black Dross Hydrothermal Treatment. *Journal of Environmental Chemical Engineering*, **1**, 23-32. <https://doi.org/10.1016/j.jece.2013.03.004>
- [18] Saifur Rahman Sarker, M.Z.A.M. and Moniruzzaman, M. (2015) Extraction and Characterization of Alumina Nanopowders from Aluminum Dross by Acid Dissolution Process. *International Journal of Minerals, Metallurgy and Materials*, **22**, 429. <https://doi.org/10.1007/s12613-015-1090-2>
- [19] Gao, W., Li, Z. and Asselin, E. (2013) Solubility of $\text{AlCl}_3 \cdot 6\text{H}_2\text{O}$ in the $\text{Fe(II)} + \text{Mg} + \text{Ca} + \text{K} + \text{Cl} + \text{H}_2\text{O}$ System and Its Salting-Out Crystallization with FeCl_2 . *Industrial & Engineering Chemistry Research*, **52**, 14282-14290.
<https://doi.org/10.1021/ie401850a>
- [20] Guo, H., Wang, J., Zhang, X., Zheng, F. and Li, P. (2018) Study on the Extraction of Aluminum from Aluminum Dross Using Alkali Roasting and Subsequent Synthesis of Mesoporous γ -Alumina. *Metallurgical and Materials Transactions B*, **49**, 2906-2916. <https://doi.org/10.1007/s11663-018-1341-5>
- [21] Hirata, Y., Fujita, H. and Shimonosono, T. (2017) Compressive Mechanical Properties of Partially Sintered Porous Alumina of Bimodal Particle Size System. *Ceramics International*, **43**, 1895-1903. <https://doi.org/10.1016/j.ceramint.2016.10.149>
- [22] How, L.F., Islam, A., Jaafar, M.S. and Taufiq-Yap, Y.H. (2017) Extraction and Characterization of γ -Alumina from Waste Aluminium Dross. *Waste and Biomass Valorization*, **8**, 321-327. <https://doi.org/10.1007/s12649-016-9591-4>
- [23] Zahir, M.H., *et al.* (2017) Microstructural Investigations of Tubular α - Al_2O_3 -Supported γ - Al_2O_3 Membranes and Their Hydrothermal Improvement. *Journal of the European Ceramic Society*, **37**, 2637-2647.
<https://doi.org/10.1016/j.jeurceramsoc.2017.02.036>
- [24] Song, P., *et al.* (2014) Preparation of Biomorphic Porous LaFeO_3 by Sorghum Straw Biotemplate Method and Its Acetone Sensing Properties. *Sensors and Actuators B: Chemical*, **196**, 140-146. <https://doi.org/10.1016/j.snb.2014.02.006>
- [25] Li, P., Guo, M., Zhang, M., Teng, L. and Seetharaman, S. (2012) Leaching Process Investigation of Secondary Aluminum Dross: The Effect of CO_2 on Leaching Process of Salt Cake from Aluminum Remelting Process. *Metallurgical and Materials Transactions B*, **43**, 1220-1230. <https://doi.org/10.1007/s11663-012-9678-7>
- [26] Vinogradov, V.V., *et al.* (2010) Sol-Gel Synthesis, Characterization and Catalytic Activity of Mesoporous γ -Alumina Prepared from Boehmite Sol by Different Methods. *Journal of Sol-Gel Science and Technology*, **56**, 333-339.
<https://doi.org/10.1007/s10971-010-2310-x>